Surface Fractal Dimension of Less-Crystalline Carbon Micropore Walls

Mutsumi Sato, Takashi Sukegawa, T. Suzuki, and Katsumi Kaneko*

Department of Chemistry, Faculty of Science, Chiba University, 1-33 Yayoi, Inage, Chiba, 263 Japan

Received: August 14, 1996; In Final Form: November 21, 1996[⊗]

The texture of pore walls of activated carbon fiber (ACF) treated at a high temperature in Ar was evaluated by surface fractal analysis using two kinds of molecular probe methods. The multiprobe (MP) method using the monolayer capacity of several different probe systems gave evidence for a decrease in the fractal dimension of the micropore walls with an increase in pretreatment temperature. As the BET monolayer gave unrealistic fractal dimension due to an erroneous evaluation of the monolayer in the micropore, this work proposed a new evaluation method of the monolayer in the micropore using the pore volume, average pore width, and molecular radius from the α_s and DR analyses. The single-probe (SP) method developed by Avnir and Jaroniec detects nitrogen and benzene adsorption isotherms. The surface fractal dimension by the MP method was between the surface fractal dimensions determined by the SP method using nitrogen and benzene. The surface fractal dimension sensitive to the probe molecule indicated the presence of irregularities of subnano order in the micropore walls.

Introduction

The surface fractal dimension[1,2] quantitatively evaluates the degree of roughness of solid surfaces. It is well-known that the surface roughness is associated with molecular processes on the solid surface. The surface fractal dimension of various solids has been determined mainly by small angle X-ray scattering (SAXS),[3−13] electron energy transfer (ET),[14−16] and adsorption.[17−38] These techniques have been applied to the evaluation of the surface fractal dimension including the pore walls. Recently the surface roughness and local surface fractal dimension of the single crystal can be observed by STM or AFM, and the relationship between the surface roughness and molecular process has been examined.[39−41] However, such a direct observation of the roughness of pore walls at an atomic level is quite difficult. The image analysis for the high-resolution transmission electron micrograph has been applied to evaluate the fractal dimension of the porous structure.[42] The molecular probe method using adsorption must play an important role in the determination of the surface fractal dimension of porous surfaces.

With the molecular probe method two methods are available for the microporous system. One is the multiprobe method (MP method),[17−32] which uses several kinds of multiprobe molecules of different molecular sizes. The MP method requires the monolayer capacity for each probe molecule. However, the MP method cannot be routinely applied to the microporous system due to a serious problem in the concept of monolayer adsorption for the microporous system.[43] We must introduce a new method in evaluation of the monolayer in the micropore. Another is the single-probe method (SP method), which was separately proposed by Avnir and Jaroniec[33,34] and Pfeifer et al.[36] The SP method should be more convenient than the MP method, but there are not many experimental examinations.[34−38]

Pfeifer and Avnir showed the principle and the availability of the MP method in 1983.[17,18] The surface fractal dimension D_{mp} is given by eq 1.

$$m = k_1\sigma^{-D_{mp}/2} \qquad 2 \le D_{mp} \le 3 \qquad (1)$$

Here, m is the monolayer capacity, σ the cross sectional area of an adsorbate, and k_1 the constant. Although the surface fractal dimension is generally expressed by D_s, this work treats two kinds of surface fractal dimension, and D_{mp} from the MP method is used. The MP method is widely applicable to various solid surfaces except for the microporous surface. If D_{mp} is 2, the surface is completely flat. The closer to 3 the D_{mp} value, the rougher the surface. Although this MP method is quite useful for the system whose monolayer capacity can be accurately determined, there has been a great argument whether the concept of monolayer adsorption is available or not in the micropore. Recent molecular simulation studies showed the presence of the monolayer adsorption process even in the micropore whose pore width is greater than the bilayer thickness of N_2 (about 0.7 nm).[44−46] Kaneko et al. showed the presence of the orientational phase transition of N_2 on the graphitic micropore wall, which is the same as the phase transition of the monolayer on the flat graphite surface.[47] Furthermore, they showed an effective method for the surface area determination in the microporous system.[48] Thus, we can determine D_{mp} using eq 1, even for micropores whose width is greater than 0.7 nm, if the monolayer evaluation fit for the micropore is introduced.

Avnir and Jaroniec derived the following relation (eq 2) using the Dubinin−Stoeckli relation[49] for the microporous carbon system.

$$\phi = k_2[\ln(P_0/P)]^{D_{sp}-3} \qquad 2 \le D_{sp} \le 3 \qquad (2)$$

where ϕ is the fractional filling at a relative pressure P/P_0 and k_2 is the constant that is defined by eq 2. In this article, this method is denoted the single-probe (SP) method, and the surface fractal dimension from the SP method is denoted by D_{sp} in this article. This equation is the same as the Frenkel−Halsay−Hill equation.[50] This relation holds well in the relative pressure range where the monolayer adsorption almost finishes on the pore walls ($P/P_0 < 0.05$). This equation leads to the surface fractal dimension D_{sp} from the single adsorption isotherm of a single probe molecule. However, the choice of the single probe should be cautious according to the pore width. A similar equation was independently proposed by Pfeifer et al.[36−38] They derived an equation applicable to mesoporous, macroporous, and flat surfaces.

The authors have tried to determine the surface fractal dimension of the less-ordered micropore walls of activated

[⊗] Abstract published in *Advance ACS Abstracts,* February 15, 1997.

S1089-5647(96)02472-8 CCC: $14.00

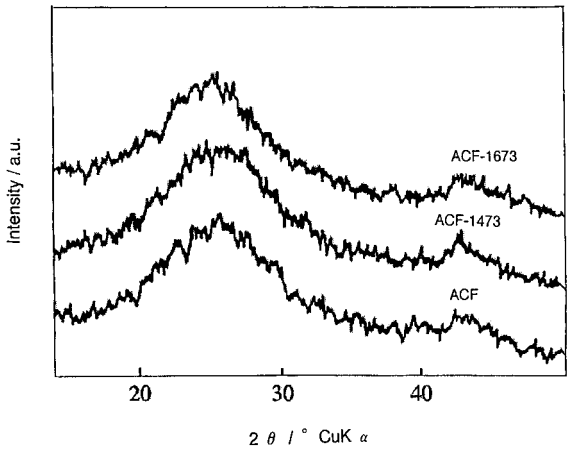

Figure 1. XRD patterns of ACFs.

carbons using the MP and SP methods and small angle X-ray scattering. We have made significant progress in understanding the micropore filling mechanism and in the separative determination of the monolayer capacity after the publication in 1991.[26] Recently, we showed a special importance of carbonaceous micropores where molecules form unusual clusters of H_2O, O_2, N_2, NO, and SO_2. The exact characterization of the slit-shaped carbon micropores is necessary for a further understanding of these molecular behaviors. Accordingly we reexamined the surface fractal dimension of the micropore walls using both of MP and SP methods. In this article the surface fractal dimension of the micropore wall roughness of activated carbon fibers heated at different temperatures in Ar is described; the difference between the methods was associated with the presence of irregularities of 1 nm and/or 0.1 nm order.

Experimental Section

Pitch-based activated carbon fibers (ACFs) and the ACFs heated in Ar for 1 h (ACF-*T*; *T* is the heating temperature) were used. The N_2 adsorption isotherms were measured by a computer-controlled gravimetric apparatus[47] at 77 K. The adsorption isotherms of the organic vapors (benzene, CH_2Cl_2, *n*-hexane, *n*-heptane, and *n*-nonane) of which molecular diameters are different from each other were measured by a volumetric high-precision adsorption apparatus[32] at 300 K. The samples were preevacuated at 383 K and 1 mPa for 2 h prior to adsorption measurements. The micrographitic structures of ACFs were investigated by X-ray diffraction using Cu Kα (45 kV, 25 mA). The X-ray photoelectron spectra were measured under <1 μPa vacuum at room temperature, using Mg Kα (6 kV, 30 mA) radiation. The binding energy was calibrated with respect to the binding energy of Au $4f_{7/2}$ (83.8 eV).

Results and Discussion

Micrographitic and Surface Functional Structures. The XRD patterns of ACFs heated at different temperatures are shown in Figure 1. The broad (002) and (10) peaks do not change with heating. The interlayer spacing d_{002} of ACFs was determined from the (002) peak position. The values of all ACFs are 0.34−0.35 nm (as shown in Table 1), being larger than that of graphite. The half-width of these peaks provides the stack height L_c and stack width L_a. These L_c and L_a values are determined using the Debye−Sherrer equation, as shown in Table 1. The micropore wall consists of two or three layers of micrographites[51] having about 7 × 7 hexagonal units, because the L_c and L_a values of these ACFs are about 0.8 and 1.8 nm, respectively.

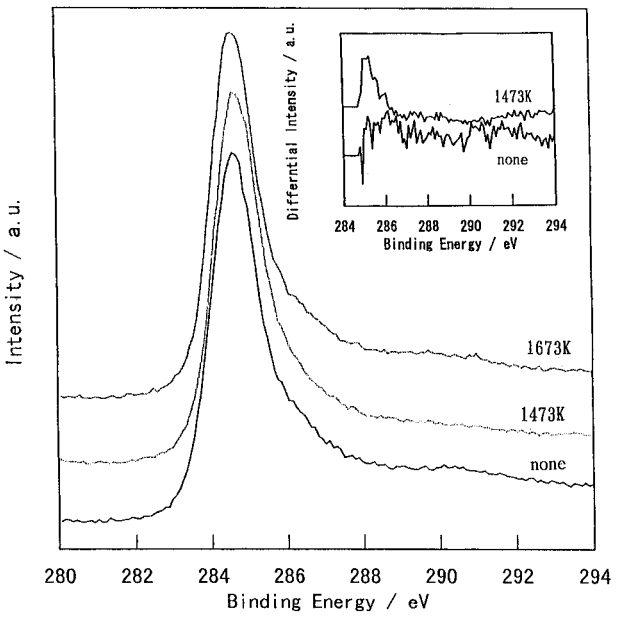

Figure 2. C 1s XPS spectral change of ACF with the high-temperature treatment.

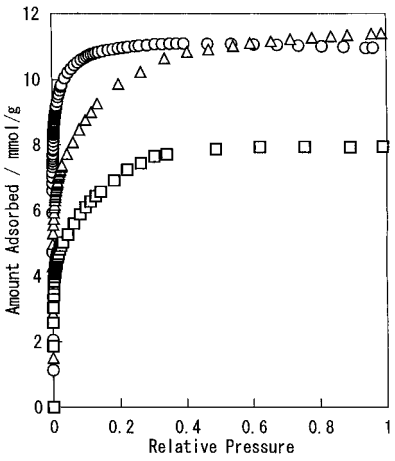

Figure 3. N_2 adsorption isotherms at 77 K: (○) ACF; (△) ACF-1473; (□) ACF-1673.

The XPS C 1s spectral changes of heat-treated ACFs are shown in Figure 2. The peak position is the same for all samples at 284.6 eV, coinciding with that of graphite. The tail region has information on surface functional groups.[52] The ACF-1673 spectrum has the lowest intensity at the high-energy side, suggesting the presence of the smallest amount of surface functional groups. The difference spectrum with the reference to ACF-1673 was determined, as shown in the inset of Figure 2. In the case of ACF-1473, there is a strong peak at 285−286 eV, which is assigned to =COH. On the other hand, ACF has two broad peaks at 285−290 and 290−294 eV. XPS studies on carbon fiber[53] reveal that =CO and −C(O)OH groups show peaks at 287 and 288.6 eV, respectively. Therefore, ACF should have =COH, =CO, and −C(O)OH groups. Thus, the heat treatment in Ar deprives these surface functional groups.

Microporosity. The nitrogen adsorption isotherms of ACFs shown in Figure 3 are of type I. The uptake curve at the low relative pressure region increases gradually with the heating temperature. Therefore, part of the micropores are widened by removal of the micrographitic layers and the surface functional groups with heating at high temperature, whereas the adsorbed amount decreases with high-temperature treatment (HTT) due to the partial consumption of the pores. Accordingly, the micropore volume and the surface area decrease with HTT. The

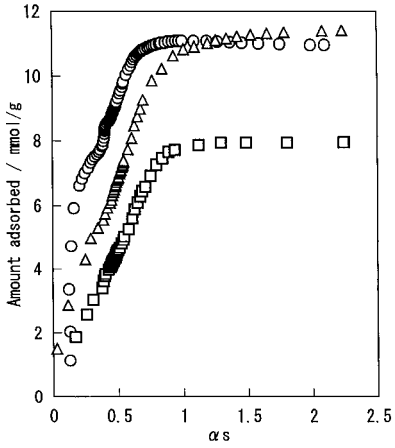

Figure 4. α_s plots of the nitrogen adsorption isotherms on ACF samples: (○) ACF; (△) ACF-1473; (□) ACF-1673.

TABLE 1: Micropore and Micrographitic Structures of ACFs from N_2 Adsorption and X-ray Diffraction

	ACF	ACF-1473	ACF-1673
total surface area/m^2 g^{-1}	996	988	783
external surface area/m^2 g^{-1}	8	5	7
total pore volume/mL g^{-1}	0.39	0.38	0.28
average pore size/nm	0.81	0.89	1.01
micropore volume/mL g^{-1}	0.40	0.38	0.29
βE_0/kJ mol^{-1}	8.0	7.5	5.6
interlayer spacing/nm	0.35	0.34	0.35
stack height/nm	0.78	0.76	0.80
stack width/nm	1.8	1.7	1.9

α_s plot was constructed for the nitrogen adsorption isotherm using the standard isotherm on the nonporous carbon black. Here α_s is defined as the ratio of the amount of adsorption at a relative pressure (P/P_0) to that at $P/P_0 = 0.4$.[50] The α_s plots of these samples are shown in Figure 4. The α_s plots for ACF and ACF-1473 have an explicit upward deviation from the linearity below $\alpha_s = 0.5$, which is ascribed to enhanced adsorption by the micropore field. As the α_s plot of ACF-1673 has no deviation, the slit width should be greater than those of ACF and ACF-1473. The total surface area, total pore volume, external surface area, and average pore width from the α_s analysis[50] are summarized in Table 1. The total surface area and the total pore volume decrease, while the external surface area and the pore width increase with HTT. Thus the micropore structure changes with HTT despite no explicit micrographitic growth. HTT should remove the surface functional groups and the imperfect micrographitic parts.

The amount of adsorption at P/P_0, W, can be associated with the adsorption potential A ($=RT \ln P/P_0$) through the Dubinin−Radushkevich (DR) equation, as given by eq 3.

$$W = W_0 \exp\{-(A/\beta E_0)^2\} \quad (3)$$

Here W_0 is the pore volume; E_0 and β are the characteristic adsorption energy and an affinity coefficient. The DR plots of ACFs are shown in Figure 5. The DR plot of ACF is linear over the whole range, but the DR plots of the heat-treated ACFs have two linear regions. The bending of both DR plots is associated with the micropore size distribution; ACF has a uniform micropore structure, but the heat-treated ACF has a micropore size distribution. The high-temperature treatment widens the micropore, as mentioned above. Thus, the high-temperature treatment gives rise to wide micropores. The micropore volume and βE_0 are summarized in Table 1. The βE_0 obtained from the DR plot at the lower relative pressure region is shown in Table 1, because the region is related to the initial micropore filling process. The βE_0 decreases with HTT. The addition of βE_0 and the enthalpy of vaporization provides the isosteric heat of adsorption $q_{st,\phi=1/e}$ at a fractional filling $\phi = e^{-1}$. Consequently, a greater βE_0 value indicates stronger adsorption in a narrower micropore. The observed order of the βE_0 value just corresponds to the decrease of the pore width, as predicted by the Dubinin−Stoeckli relationship.[50]

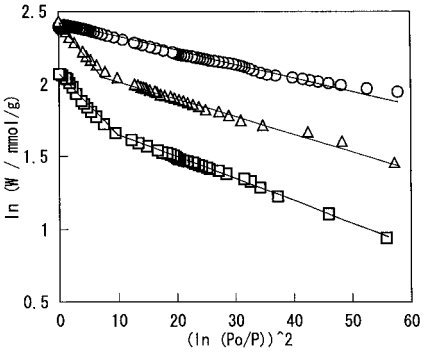

Figure 5. DR plots of the nitrogen adsorption isotherms on ACF samples: (○) ACF; (△) ACF-1473; (□) ACF-1673.

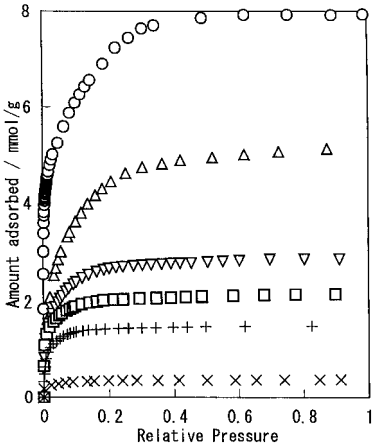

Figure 6. Adsorption isotherms of various vapor molecules on ACF-1673: (○) N_2; (△) CH_2Cl_2; (▽) benzene; (□) *n*-hexane; (+) *n*-heptane; (×) *n*-nonane.

Evaluation of the Monolayer Capacity for an Organic Molecule. The adsorption isotherms of nitrogen and organic vapors for ACF-1673 are shown in Figure 6. All isotherms other than that for nonane are of type I, suggesting that adsorption proceeds by micropore filling. The adsorption amount was greater as the molecular size decreased. In the case of ACF, the adsorption amount of nitrogen was much greater than the adsorbed amount of other molecules. The difference in the amount of adsorption with the size difference of probe molecules indicates a change of the surface fractal structure with the heating temperature.

Evaluation of the surface fractal dimension D_m with the MP method requires both the molecular cross sectional area σ and the monolayer capacity for each probe molecule. The σ value was calculated from the bulk liquid density. The monolayer capacity, m, has been obtained by the BET method for the meso- or macroporous surfaces. The monolayer capacity from the BET plot is expressed by m_B in this report. As the BET method cannot be routinely applied to the micropore, we propose another method for the estimation of the monolayer capacity m_S. The micropores are slit-shaped, and the probe molecules from an adsorbed layer structure in the slit-pore of constant width can be determined by the α_s analysis for the nitrogen adsorption isotherm. The m_S for each probe molecule can be calculated from the average pore width w, pore volume V, and molecular

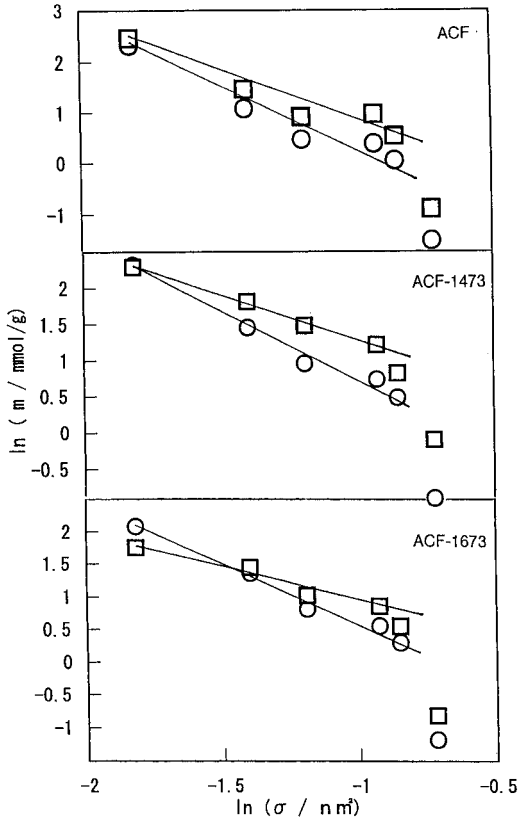

Figure 7. ln σ vs ln m plots for ACF samples: (○) m_B; (□) m_G.

TABLE 2: Surface Fractal Dimensions D_{mp} and D_{sp} of ACFs

	ACF	ACF-1473	ACF-1673
D_{mp} from m_S	2.7	2.6	2.3
D_{mp} from m_B	4.4	3.7	3.3
D_{sp} from nitrogen	2.8	2.6	2.5
D_{sp} from benzene	2.5	2.4	2.3

diameter d that is calculated from bulk liquid density.

$$m_S = 2V/(w/d) \quad (4)$$

Here, the pore volume V is obtained from the DR analysis. The determined m_S means the average molecular number for covering the micropore walls with a single adsorbed layer.

Surface Fractal Dimension from the MP Method. The logarithmic plots of eq 1 for ACFs are shown in Figure 7. All plots are linear except for the point of the greatest probe molecule, nonane. Both m_B and m_S give a good linear relation. The slope of the line from m_S is smaller than that from m_B. The surface fractal dimensions D_{mp} from m_S and m_B are summarized in Table 2. The D_{mp} value from m_B is more than 3, which is ascribed to an imperfect monolayer formation near the B point. On the contrary, the m_S value provides a reasonable D_{mp} value, because the m_S is not affected by the adsorbed state near the B point. We believe that the D_m from m_S has a physical meaning. The D_m value decreases with HTT, suggesting that the micropore wall becomes flatter with HTT. As the D_m value of 2.3 for ACF-1673 is greater than that of graphite (2.1),[32] even the micropore wall of ACF-1673 has irregularities mainly around the intermicrographitic junction.

Surface Fractal Dimension from the SP Method. N_2 and benzene adsorption isotherms of ACFs are shown in Figures 3 and 8, respectively. In the case of N_2 adsorption, the amount of adsorption on the original ACF is the greatest of the three ACFs. On the contrary, the amount of benzene adsorption on the original ACF is the smallest. This reversal behavior comes from the micropore wall structure having different surface fractal dimension. Therefore, we can expect that SP methods for

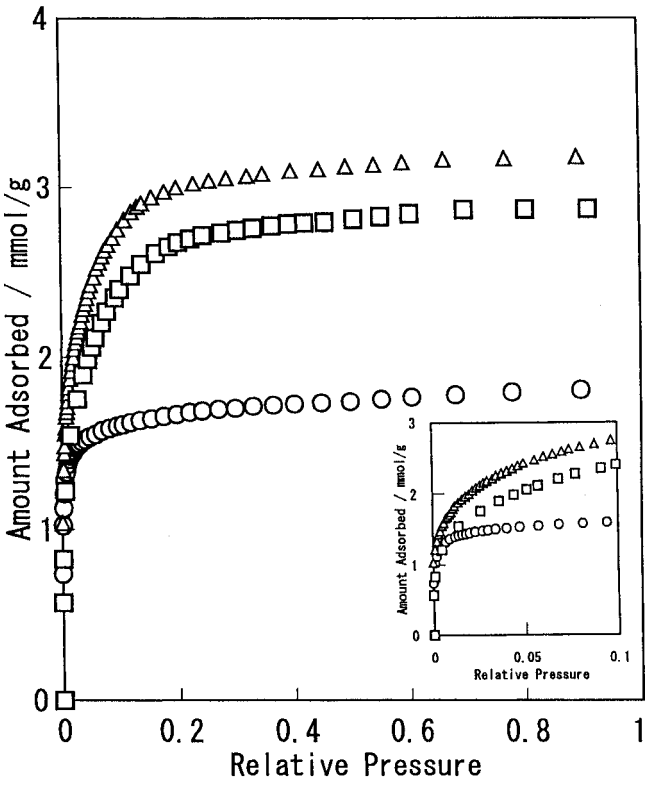

Figure 8. Adsorption isotherms of benzene on ACF samples at 300 K: (○) ACF; (△) ACF-1473; (□) ACF-1673.

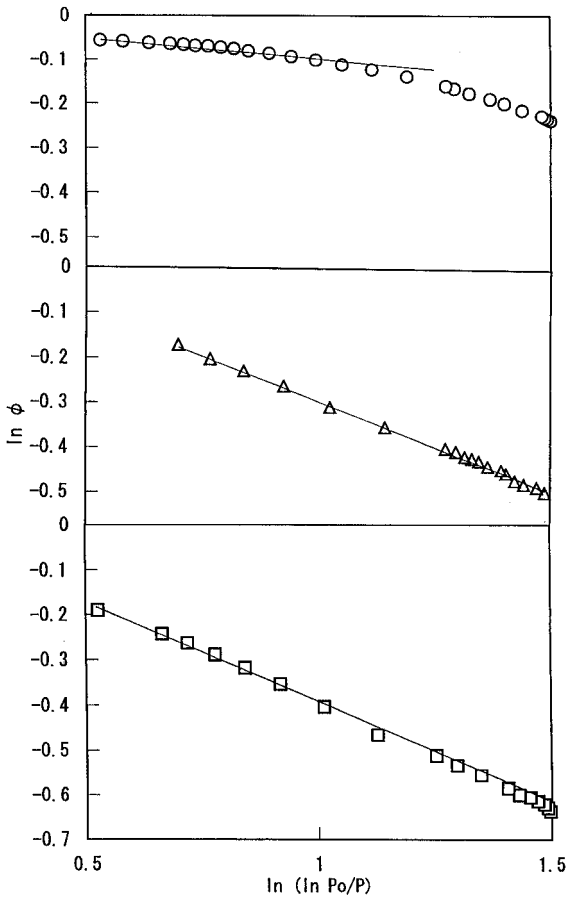

Figure 9. ln ϕ vs ln(ln P_0/P) plots for the nitrogen adsorption isotherms of ACF samples: (○) ACF; (△) ACF-1473; (□) ACF-1673.

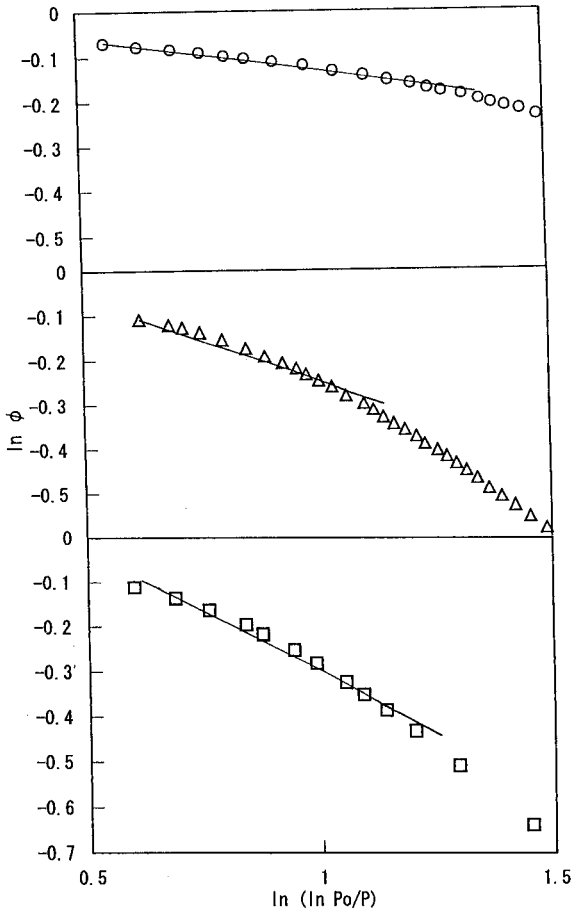

Figure 10. ln ϕ vs ln(ln P_0/P) plots for the benzene adsorption isotherms of ACF samples: (○) ACF; (△) ACF-1473; (□) ACF-1673.

nitrogen and benzene provide important information on the roughness of the micropore walls.

The ln ϕ vs ln(ln(P/P_0)) plot was applied to the adsorption data near $P/P_0 = 0.05$, where micropore filling almost finishes. Figure 9 shows the ln ϕ vs ln(ln(P/P_0)) plot for the nitrogen adsorption isotherm on three ACFs. All plots are good lines. The slope of the plot becomes smaller with the increase of HTT, leading to the surface fractal dimension D_{sp}. The D_{sp} value is in the range 2.5−2.8, as shown in Table 2. This agrees well with the result by the MP method. In a similar way, we applied the ln ϕ vs ln(ln(P/P_0)) plot to the benzene adsorption isotherm, as shown in Figure 10. Although the linearity is not good compared with nitrogen, D_{sp} from benzene was estimated from the linear section. The obtained D_{sp} value from benzene is in the range 2.3−2.5, which is smaller than that from nitrogen. This difference indicates that the SP method can evaluate sensitively the structural causes for the surface fractal nature. Although the difference in the average molecular size between benzene and nitrogen is only 0.06 nm, the D_s value depends strongly on the probe size. Strictly speaking, the difference in the probe molecule−pore wall interaction should affect the observed behavior, too. Thus this SP method using different probes is quite helpful in understanding the fine pore wall structure at an atomic level. Figure 11 shows the changes of the surface fractal dimension with HTT. The surface fractal dimension decreases with HTT, as suggested in the pioneering works.[18,29] The D_{mp} from the MP method, D_{sp} from the SP method with nitrogen $D_{sp}(N_2)$, and D_{sp} from the SP method with benzene D_{sp}(benzene) are shown in Figure 11. Though the benzene molecule is not the greatest of these probe molecules, D_{mp} is situated between $D_{sp}(N_2)$ and D_{sp}(benzene). As the SP method using a larger probe molecule is not fit for evaluation,

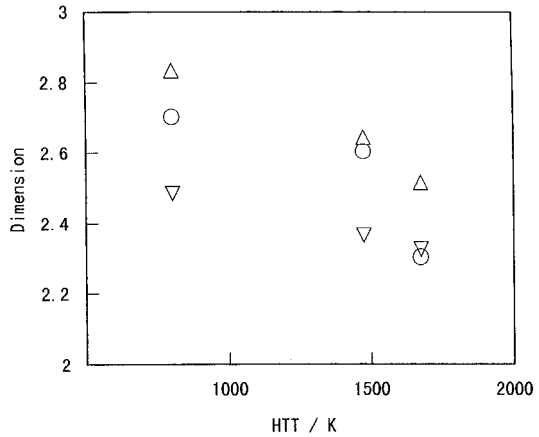

Figure 11. Surface fractal dimension vs HTT: (○) D_{mp}; (△) $D_{sp}(N_2)$; (▽) D_{sp}(benzene).

the surface fractal dimension should be underestimated. However, the difference of D_{sp} from different probes provides important information on the pore wall structure.

The Structural Change of the Carbon Micropore. The micropores in ACF stem from mainly the slit-shaped voids between micrographites. Strictly speaking, the void is not a regular slit, but wedge-shaped. Also a cagelike void surrounded by intermicrographite bonds should contribute to the micropore. The surface functional groups should be situated at the intermicrographite junctions, giving rise to the rough pore wall. High-temperature heating should remove the irregular structures in the imperfect basal plane of the micrographite wall. Hence the change in the surface fractal dimension can be associated with these structure changes. If micrographites have regular basal planes and they have a mutually parallel oriented structure of no micropores at the intermicrographite junctions, the surface fractal dimension of the micropore wall must be close to 2.

The X-ray diffraction showed that HTT does not change the c-spacing and it does not clearly increase the L_c. Accordingly the micrographitic unit structure is preserved even after HTT. According to the previous work,[51] the diamagnetism becomes more marked due to HTT, indicating the extension of the π-electron-conjugated system. The micrographites of the original ACF should have irregularities such as defaults in imperfect basal planes; HTT removes these irregularities, but the micrographite still does not grow.[52] As the surface functional groups at the junctions of the micrographites are detached by HTT, the irregular wedge-shaped pores and cagelike voids develop, providing greater micropores having smoother pore walls. Thus, HTT should reduce the roughness due to the intermicrographite junctions. Also the decrease of $q_{st,\phi=1/e}$ with HTT supports the change of the surface fractal dimension, since the irregularities at the micrographite junction and on the basal plane should have enough size to interact with the probe molecule. Accordingly, the surface fractal analysis can well characterize even the micropore walls under the requirements proposed in this work.

Acknowledgment. This work was supported in part by the Grant-in-Aid for Scientific Research on Priority Areas (Carbon Alloys) from the Ministry of Education, Culture, and Science, Japanese Government.

References and Notes

(1) Mandelbrot, B. B. *The Fractal Geometry of Nature*; Freeman: San Francisco, 1982.
(2) Takayasu, H. *Furakutaru*; Asakura syoten: Tokyo, 1986.
(3) Bale, H. D.; Schmidt, P. W. *Phys. Rev. Lett.* **1984**, *53*, 596.

(4) Craievich, A.; Aegerter, M. A.; dos Santos, D. I.; Woignier, T.; Zarzycki, J. *J. Non-Cryst. Solids* **1987**, *86*, 394.
(5) dos Santos, D. I.; Aegerter, M. A.; Craievich, A.; Lours, T.; Zarzycki, J. *J. Non-Cryst. Solids* **1987**, *95* and *96*, 1143.
(6) Höhr, A.; Neumann, H. B.; Schmidt, P. W.; Pfeifer, P.; Avnir, D. *Phys. Rev. B* **1988**, *38*, 1462.
(7) Schmidt, P. W.; Höhr, A.; Neumann, H. B.; Avnir, D.; Lin, J. S. *J. Chem. Phys.* **1989**, *90*, 5016.
(8) Klafter, J.; Nlumen, A. *J. Chem. Phys.* **1984**, *80*, 875.
(9) Rojanski, D.; Huppert, D.; Bale, H. D.; Decai, X.; Schmidt, P. W.; Farin, D.; Seri-Levy, A.; Avnir, D. *Phys. Rev. Lett.* **1986**, *56*, 2505.
(10) Snook, I.; Mcmahon, P. *Langmuir* **1993**, *9*, 2726.
(11) Beddoe, R. E.; Lang, K. *Cem. Concr. Res.* **1994**, *24*, 605.
(12) Brennan, A. B.; Miller, T. M. *Chem. Mater.* **1994**, *6*, 262.
(13) Skatov, L. I.; Konotop, V. V.; Cheremskoi, P. G.; Gomozov, V. P.; Bairachnyi, B. I. *Phys. Chem. Mech. Surf.* **1995**, *9*, 907.
(14) Pines, D.; Huppert, D. *J. Phys. Chem.* **1987**, *91*, 6569.
(15) Pines, D.; Huppert, D.; Avnir, D. *J. Chem. Phys.* **1988**, *89*, 1177.
(16) Pines, D.; Huppert, D. *J. Chem. Phys.* **1989**, *91*, 7291.
(17) Pfeifer, P.; Avnir, D. *J. Chem. Phys.* **1983**, *79*, 3558.
(18) Avnir, D.; Farin, D.; Pfeifer, P. *J. Chem. Phys.* **1983**, *79*, 3558.
(19) Avnir, D.; Farin, D.; Pfeifer, P. *J. Colloid Interface Sci.* **1985**, *103*, 112.
(20) Farin, D.; Pelog, S.; Yavin, D.; Avnir, D. *Langmuir* **1985**, *1*, 399.
(21) Myer, A. Y.; Farin, D.; Avnir, D. *J. Am. Chem. Soc.* **1986**, *108*, 7897.
(22) Avnir, D. *J. Am. Chem. Soc.* **1987**, *109*, 2931.
(23) Farin, D.; Avnir, D. *J. Phys. Chem.* **1987**, *91*, 5517.
(24) Farin, D.; Avnir, D. *J. Am. Chem. Soc.* **1988**, *110*, 2039.
(25) Ludlow, D. K.; Moberg, T. P. *Anal. Instrum.* **1990**, *19*, 113.
(26) Kaneko, K. *Langmuir* **1991**, *7*, 109.
(27) Neimark, A. V. *Adsorpt. Sci. Technol.* **1990**, *7*, 210.
(28) Lefebvre, Y.; Lacelle, S.; Jolicoeur, C. *J. Mater. Res.* **1992**, *7*, 1888.
(29) Avnir, D.; Farin, D.; Pfeifer, P. *New J. Chem.* **1992**, *16*, 439.
(30) Conner, W. C.; Bennett, C. O. *J. Chem. Soc., Faraday Trans.* **1993**, *89*, 4109.
(31) Sato, M.; Sukegawa, T.; Suzuki, T.; Hagiwara, S.; Kaneko, K. *Chem. Phys. Lett.* **1991**, *181*, 526.
(32) Avnir, D.; Jaroniec, M. *Langmuir* **1989**, *5*, 1431.
(33) Jaroniec, M.; Lu, X.; Maday, R.; Avnir, D. *J. Chem. Phys.* **1990**, *92*, 7589.
(34) Ehrburger-Dolle, F.; Holz, M.; Lahaye, J. *Pure Appl. Chem.* **1993**, *65*, 2223.
(35) Kaneko, K.; Sato, M.; Suzuki, T.; Fujiwara, Y.; Nishikawa, K.; Jaroniec, M. *J. Chem. Soc., Faraday Trans.* **1991**, *87*, 179.
(36) Pfeifer, P.; Wu, Y. J.; Cole, M. W.; Krim, J. *Phys. Rev. Lett.* **1989**, *62*, 1997.
(37) Pfeifer, P.; Cole, M. W. *New J. Chem.* **1990**, *114*, 221.
(38) Ismail, I. M. K.; Pfeifer, P. *Langmuir* **1994**, *10*, 1532.
(39) Ocon, P.; Herrasti, P.; Vara, J. M.; Vazquez, L.; Salvarezza, R. C.; Arvia, A. J. *J. Phys. Chem.* **1994**, *98*, 2418.
(40) Palasantzas, G. *Phys. Rev. B* **1994**, *49*, 10544.
(41) Iwasaki, H.; Yoshinobu, T. *Phys. Rev. B* **1993**, *48*, 8282.
(42) Oshida, K.; Endo, M.; di Vittorio, S. L.; Dresselhaus, M. S.; Dresselhaus, G. *J. Mater. Res.* **1993**, *8*, 512.
(43) Sing, K. S. W.; Evert, D. H.; Haul, R. A. W.; Mosocou, L.; Pierotti, R. A.; Rouquerol, J.; Siemieniewska, T. *Pure Appl. Chem.* **1985**, *57*, 603.
(44) Kaneko, K.; Cracknell, R. F.; Nichlson, D. *Langmuir* **1994**, *10*, 4606.
(45) Cracknell, R. F.; Gordon, P.; Gubbins, K. E. *J. Phys. Chem.* **1993**, *97*, 494.
(46) Suzuki, T.; Kaneko, K.; Setoyama, N.; Maddox, M.; Gubbins, K. E. *Carbon* **1996**, *34*, 909.
(47) Kaneko, K.; Suzuki, T.; Kakei, K. *Langmuir* **1989**, *5*, 879.
(48) Kaneko, K.; Ishii, C. *Colloids Surf.* **1992**, *67*, 203.
(49) Dubinin, D. *Chem. Rev.* **1990**, *60*, 235.
(50) Gregg, S. J.; Sing, K. S. W. *Adsorption, surface area and porosity*, 2nd ed.; Academy Press: London, 1982.
(51) Iiyama, T.; Nishikawa, K.; Otowa, T.; Kaneko, K. *J. Phys. Chem.* **1995**, *99*, 10075.
(52) Kanoh, H.; Kaneko, K. *J. Phys. Chem.* **1996**, *100*, 755.
(53) Kaneko, K.; Shimizu, K.; Suzuki, T. *J. Chem. Phys.* **1992**, *98*, 8705.
(54) Imai, J.; Souma, M.; Ozeki, S.; Suzuki, T.; Kaneko, K. *J. Phys. Chem.* **1991**, *95*, 9955.
(55) Wang, Z. W.; Kaneko, K. *J. Phys. Chem.* **1995**, *99*, 16714.
(56) Kaneko, K. *Colloids Surf.* **1996**, *109*, 319.
(57) Kaneko, K.; Yamaguchi, K.; Ishii, C.; Ozeki, S.; Hagiwara, S.; Suzuki, T. *Chem. Phys. Lett.* **1991**, *176*, 75.
(58) Kaneko, K.; Ohbu, K.; Uekawa, N.; Kaneko, K. *Langmuir* **1995**, *11*, 728.
(59) Takahagi, T.; Ishitani, A. *Carbon* **1984**, *22*, 43.